

## Generation of tomographic measurement data of mesoscopic quantum states

JULIAN GÖTTSCHE,<sup>1</sup> STEPHAN GREBIEN,<sup>1</sup>  FELIX PEIN,<sup>1</sup> MALTE LAUTZAS,<sup>1</sup> DANIELA ABDELKHALEK,<sup>1</sup> LORENA REBÓN,<sup>1,2</sup>  BORIS HAGE,<sup>3</sup> JAROMÍR FIURÁŠEK,<sup>4</sup>  AND ROMAN SCHNABEL<sup>1,\*</sup> 

<sup>1</sup>Institut für Quantenphysik & Zentrum für Optische Quantentechnologien, Universität Hamburg, Luruper Chaussee 149, 22761 Hamburg, Germany

<sup>2</sup>Instituto de Física La Plata, Universidad Nacional de La Plata, 1900 Buenos Aires, Argentina

<sup>3</sup>Institut für Physik, Universität Rostock, 18051 Rostock, Germany

<sup>4</sup>Department of Optics, Faculty of Science, Palacký University, 17. listopadu 12, 77900 Olomouc, Czech Republic

\*roman.schnabel@uni-hamburg.de

Received 13 March 2025; revised 9 June 2025; accepted 26 June 2025; published 28 July 2025

Microscopic Schrödinger cat states are generated from quantum-correlated fields using a probabilistic heralding photon subtraction event. Subsequent quantum state tomography provides complete information about the state, revealing numbers of quantum-correlated photons of the order of one. Optical quantum computing requires even more sophisticated states with significantly higher photon numbers. Here, we present a concept to derive tomographic “measurement” data of states with average quantum-correlated photon numbers significantly larger than one without having these states available. We generate a photon-subtracted squeezed vacuum state of light and simultaneously measure a pair of orthogonal field quadratures. Subsequent data post-processing emulates the optical interference of two copies. One of the interference results is accepted as the new “measurement” value if the second interference result falls below a threshold value. Evaluating the final tomographic data shows that two iterations of the breeding protocol increase the mean photon number of the state from  $\approx 1$  to  $\approx 4$ . Our concept for obtaining tomographic measurement data of mesoscopic non-classical states that physically never existed provides a way to benchmark future quantum technologies.

© 2025 Optica Publishing Group under the terms of the [Optica Open Access Publishing Agreement](#).

<https://doi.org/10.1364/OPTICAQ.562217>

### 1. INTRODUCTION

Stationary fields with quantum correlations and long coherence times are resources of quantum sensing [1,2], quantum communication [3,4], and quantum computing [5–7]. In general, the realization of a greater quantum advantage requires a larger (average) number of quantum-correlated photons  $n_{qc}$  in the state used. Increasing  $n_{qc}$  by “breeding,” which converts several copies of the input state into one more complex state such as a cat-like state with higher amplitude or a state closer to the ideal Gottesman–Kitaev–Preskill state [8–10], is currently a highly active topic in the context of optical quantum computing. The recent construction of a hardware scale model, however, revealed a significant gap between present-day performance and the demands of fault-tolerant quantum computing [7]. In the current situation, it would be useful to have an approach available with which hardware scaling models could be benchmarked in terms of their achievable performance in principle. The idea of benchmarking quantum technologies has been considered before [11]; however, there is no benchmarking concept to date that provides

complete measurement data of an ensemble of grown states after breeding without having to set up the entire hardware for the breeding protocol.

Squeezed vacuum states of diffraction-limited laser beams are the most fundamental quantum-correlated optical resource. Their number of quantum-correlated photons is given by  $n_{qc} = (\beta + 1/\beta)/4 - 0.5$  [12], where  $\beta = \Delta^2 \hat{X}_{vac} / \Delta^2 \hat{X}_\theta$  is the measurable squeeze factor,  $\Delta^2 \hat{X}_{vac}$  is the variance of the ground state uncertainty of the electromagnetic field,  $\Delta^2 \hat{X}_\theta$  is the variance of the most squeezed quadrature, and  $\theta$  is the squeeze angle. The highest measured squeeze factor so far is  $\beta \approx 32$ , which corresponds to approximately 15 dB [13] and  $n_{qc} \approx 7.4$  without any heralding signal or any other conditional detection event. Individual values of the field quadratures  $X_{vac,i}$  and  $X_{\theta,i}$  are measured with balanced homodyne detection in a continuous fashion. Field quadratures of different angles (modulo  $\pi$ ) do not commute. Orthogonal quadratures are often named  $\hat{X}$  and  $\hat{Y}$ . They obey a Heisenberg uncertainty relation and span a phase space for quasi-probability density distributions such as

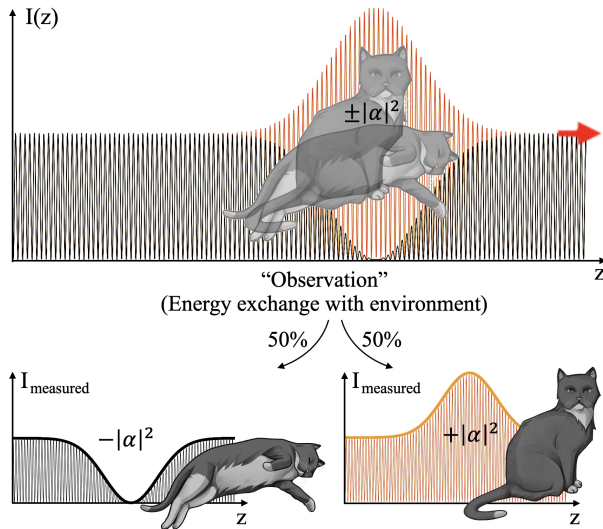


**Fig. 1. Illustration of an optical Schrödinger cat**—Optical wave packets simultaneously constructively and destructively interfere with an optical local oscillator beam. The intensity measurement  $I_{\text{measured}}$  would show either a bright or a dark pulse with a “quantum-random” probability of 50% each. Quantum randomness can be *certified* by measuring two non-commuting quadratures of the optical field  $\hat{X}$  and  $\hat{Y}$ . The tomographically reconstructed Wigner function proves a Schrödinger cat state including its macroscopicity  $|\alpha|^2$  (brightness) and degradation due to decoherence. Different from previous works [17–20], we measure on each copy of the state the two non-commuting field strengths *simultaneously* resulting in observables that we name  $\hat{X}^Q$  and  $\hat{Y}^Q$ .

the Wigner function. The Wigner function is reconstructed from subsequent (tomographic) ensemble measurements of  $\hat{X}$  and  $\hat{Y}$ , with one of them identical to  $\hat{X}_\theta$  [14].

While squeezed states have an entirely positive Wigner function [15], states with partially negative quasi-probability densities can be produced from them by the probabilistic subtraction of a single photon [16]. The subtraction event can be used as a heralding trigger that enables tomographic ensemble measurements of  $\hat{X}$  and  $\hat{Y}$ . For a weakly squeezed input state, the output state approximately corresponds to a *microscopic* Schrödinger cat state having an average photon number of the order of one [17–20]. Figure 1 illustrates the physical concept of an optical Schrödinger cat state, which, in theory, can be made of an arbitrarily high number of quantum-correlated photons.

In order to go beyond microscopic Schrödinger cat states in the experiment, it was proposed to superimpose two copies of these states on a beam splitter and to exploit the fact that a grown Schrödinger cat state can be probabilistically generated at one output by conditioning on suitable measurement outcome on the other beam splitter output that serves as a heralding trigger [21]. Figure 2(a) illustrates the probabilistic growing protocol. So far, only one growing step was realized [9,10]. In [9], the size of a generated Schrödinger cat state increased from about 1.3 to about 3.4. Due to their detection efficiency of just 62%, the actually measured size increased from  $|\alpha_0|^2 \approx 0.8$  to  $|\alpha_1|^2 \approx 2.1$ . Larger such states are the goal of highly active research in optical quantum computing [6,7]. For this work, we define a quantum-correlated state as *mesoscopic* if the number of its quantum-correlated photons  $n_{\text{qc}}$  is ten or more. The highest numbers of quantum-correlated photons per state to date of up

to  $n_{\text{qc}} = 8$  have been measured in photon counting experiments when only time windows were analyzed in which the desired number of photons was actually measured [22,23]. This concept does not allow any heralding for use in an optical downstream protocol.

Here, we report the proof of principle of a new experimental concept for the generation of tomographic measurement data on *mesoscopic* Schrödinger cat states. The innovative part of our setup is the tomographic measuring device, which is composed of two balanced homodyne detectors *simultaneously* measuring two orthogonal non-commuting field quadratures  $X_{\text{mode}}^Q$  and  $Y_{\text{mode}}^Q$  on every single copy of a heralded microscopic Schrödinger cat state produced by a single source. We propose to use emulation of iterative multi-step breeding of Schrödinger cat states for precise benchmarking of quantum technologies in the regime of mesoscopic states.

The uncertainty product of *simultaneously* measured orthogonal field quadratures  $X_{\text{mode}}^Q$  and  $Y_{\text{mode}}^Q$  is bounded from below by a Heisenberg-uncertainty-type relation but with the lower bound doubled [24]. The measuring device that we use in an innovative way has been called “eight-port homodyne detector” [25] or “heterodyne detector” [26]. Here, we introduce the term “Q-function homodyne detector” (QHD) because we consider it more descriptive and less ambiguous than the previous terms. “QHD” is known to directly provide the Husimi Q-function [27], and thus the full ensemble information. We can thus apply data post-processing that *emulates* optical two-copy interference of the state on a virtual balanced beam splitter (with perfect interference contrast). One of the two tomographic (complex-valued) interference outputs is accepted as a new tomographic “measurement” value, if the second interference output falls below a threshold value. The Q-function of the new ensemble data represents measurement results as would be obtained by measuring a Schrödinger cat state with a grown photon number. No “post-selection” takes place, as we do not make the new “measurement” data dependent on the output state of our protocol with a grown photon number. The generated “measurement” data is indistinguishable from actual measurement data on an ensemble of this state, although this ensemble has not physically existed as an optical ensemble at any time. Figure 2(b) illustrates our concept and compares it with the conventional hardware-based concept shown in (a). Evidently, our approach requires the complete measurement of the existing optical states, similar to the conditional measurement data generation in [22,23]. Heralding the grown state is not possible.

## 2. EXPERIMENT AND ANALYSIS

Figure 3 shows the schematic of our laser setup used for the generation of a microscopic optical Schrödinger cat state, similar to [18]. Every such state was generated probabilistically, heralded by a detection event  $j$  of a super-conducting nanowire single-photon detector (SPD) having a quantum efficiency of greater than 93% at 1064 nm. Altogether, we measured  $1.2 \times 10^9$  time modes around heralding events being in the same microscopic Schrödinger cat state in about three and a half hours.

The innovation of our experiment was the *simultaneous* measurement of two orthogonal, non-commuting field quadratures  $X_{\text{mode},j}^Q$  and  $Y_{\text{mode},j}^Q$ , whose simultaneous precision is bounded by a Heisenberg uncertainty relation. This “Q-function homodyne detection” (QHD) allows for data-based production of

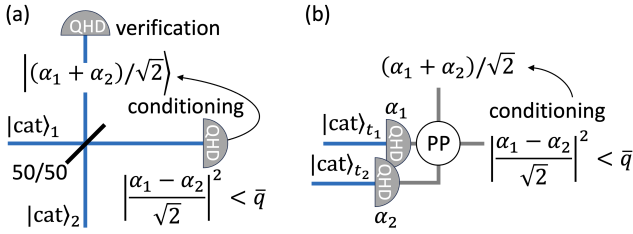


**Fig. 2. Schrödinger cat growing protocols**—(a) Traditional hardware-based protocol for producing from two copies of a microscopic cat state a grown one for downstream applications [9,21]. The two copies must be available at the same time in order to overlap optically on a balanced beam splitter. Each copy is produced individually and probabilistically. One beam splitter output is measured in the coherent state basis by Q-function homodyne detection (QHD). A grown cat state is heralded if the measured value is below a threshold value, which indicates projection onto a coherent state sufficiently close to the vacuum state. (b) Our protocol for producing “measurement” data of grown cat states. A single source continuously produces copies of a microscopic cat state, which are measured by a single Q-function homodyne detector (QHD) at subsequent times. The QHD projects each copy onto two real values  $X_{\text{mode},j}^Q$  and  $Y_{\text{mode},j}^Q$  with  $\alpha_j = X_{\text{mode},j}^Q + iY_{\text{mode},j}^Q$ . Post-processing (PP) emulates the superposition on a beam splitter for two copies ( $j \in \{1, 2\}$ ). The PP probabilistically provides measurement data of a grown cat state as the verification in the hardware-based protocol would do, however, an arbitrary amount of iterative growing steps is straight forward. The only requirement is that the measurement time has been long enough to generate a sufficiently large ensemble. The two protocols are equivalent even if realistic detectors with detection efficiency  $\eta < 1$  are employed, provided that the detection efficiency is identical for all detectors.

“measurement” data from a larger than actually available Schrödinger cat state. Before we come to this, we describe our result on the measurement of the initial microscopic Schrödinger cat state, where we do not apply any correction, e.g., the imperfect quantum efficiency of the detection.

The ensemble of the pairs contained the full information about the Schrödinger cat state, which is conflated by the Husimi Q-function shown in Fig. 4 (top left). The bottom left shows the corresponding Wigner function, which we calculated from the Q-function. In principle, this can be achieved by deconvolving the Q-function with the Gaussian function describing the ground state uncertainty, but this procedure amplifies noise and other imperfections. To derive the tomographic reconstructions in the Wigner representation without deconvolution of the Q-functions, we first reconstructed the states’ density matrices in Fock basis. For this, we divided the phase space into  $K = 120^2$  rectangular bins with area  $d^2$  and counted the number of measurement outcomes  $f_k$  in each bin  $k$ . We associated a positive operator valued probability measure (POVM) element  $\hat{\Pi}_k = \frac{d^2}{\pi} |\alpha_k\rangle\langle\alpha_k|$  with each bin, where  $\alpha_k$  was the complex amplitude at the center of the bin. We employed the maximum-likelihood quantum state tomography and sought the density matrix  $\hat{\rho}$  that maximized the likelihood function

$$\mathcal{L} = \prod_{k=1}^K (\text{Tr}[\hat{\Pi}_k \hat{\rho}])^{f_k}$$

under the constraints  $\hat{\rho} \geq 0$  and  $\text{Tr}[\hat{\rho}] = 1$ . In the numerical calculations, we truncated the Fock space at photon number  $N = 20$ .

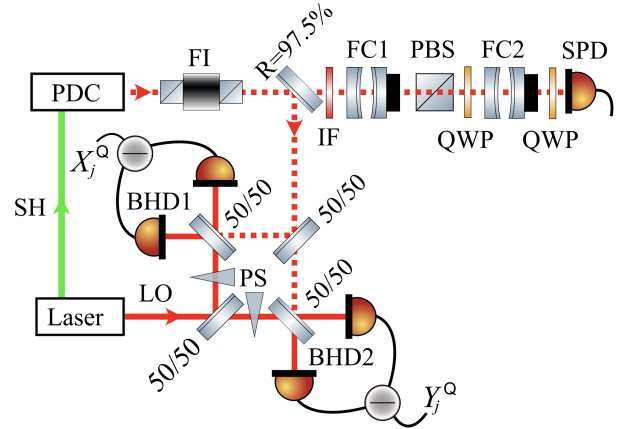


**Fig. 3. Laser interferometric setup**—Second harmonic (SH) light at 532 nm pumps degenerate parametric down-conversion (PDC) inside a crystal to stationary produce states with squeezed uncertainty at 1064 nm. Using interference with a 1064 nm local oscillator (LO), two balanced homodyne detectors (BHD1/2) continuously and simultaneously measure the field quadratures with the anti-squeezed electromagnetic field uncertainty  $X^Q$  and with the squeezed one  $Y^Q$  on 97.5% of the states. If the single photon detector (SPD) registers a photon “ $j$ ,” the  $X_j^Q$  and  $Y_j^Q$  values in the corresponding time window belong to a microscopic Schrödinger cat state. The measured probability distribution of a typical ensemble is shown in Fig. 4 (top left). FC1, FC2, filter cavities of different lengths for matching the measurement spectrum of the SPD to that of the BHDs; FI, Faraday isolator; IF, interference filter; PBS, polarizing beam splitter; PS, phase shifter; QWP, quarter wave plate to suppress coupling of FC1 and FC2 and provide optimal polarization for the SPD.

Starting from a maximally mixed state in the truncated Fock space, the density matrix that maximizes  $\mathcal{L}$  can be determined by repeated iterations of the following non-linear map [28–30]:

$$\hat{\rho} \rightarrow \frac{\hat{R} \hat{\rho} \hat{R}^\dagger}{\text{Tr}[\hat{R} \hat{\rho} \hat{R}^\dagger]}, \quad \text{with } \hat{R} = \sum_{k=1}^K \frac{f_k}{\text{Tr}[\hat{\Pi}_k \hat{\rho}]} \hat{\Pi}_k.$$

The Wigner functions plotted in Fig. 4 were calculated from the reconstructed density matrices in Fock basis. The Wigner function is the quasi-probability density function that describes the conventional ensemble measurement, where the ensemble is split into two to measure the two orthogonal quadratures separately, i.e., without splitting the states. The two representations on the left in Fig. 4 are clearly that of a Schrödinger cat state because they show two well-separated maxima with opposite signs along one of the field quadratures, and the Wigner function shows negativities in between. The opposite sign describes the fact that the state simultaneously interferes constructively and destructively with a coherent state displaced along the same field quadrature, resembling Fig. 2. The negativities prove that the measured state is not simply a mixed state of either a positive or a negative sign, and we can conclude that the representations in Fig. 4 left describe every single ensemble member. Note that the existence of local hidden variables that nevertheless would allow to divide the states into different subclasses was ruled out by the experimental violations of Bell inequalities [31–33].

Several important parameters of the generated photon-subtracted squeezed state are listed in Table 1. This table includes the mean photon number  $\bar{n} = \langle \hat{n} \rangle$  of the state, its purity

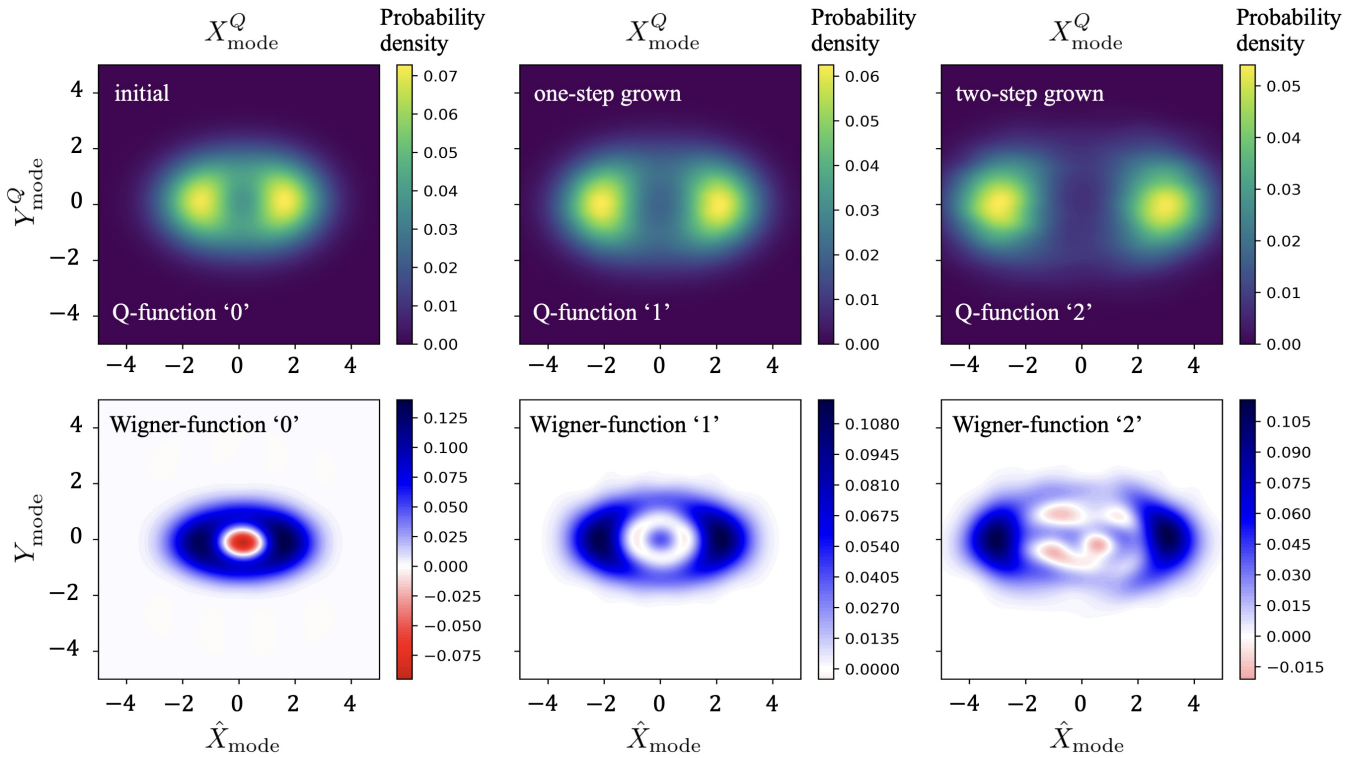


**Fig. 4. Tomography results (without corrections)**—Top row: Q-functions as directly derived from the measured data points (left) and the data points produced by measurements plus post-processing (center and right) and smoothed with Kernel density estimation. Bottom row: Wigner functions derived from the Q-function data. Left column: Initial Schrödinger cat state with a negativity value of  $W_{\min,0} = -0.093$  and mean photon number  $\approx 1.08$ . The deeper the negativity, the more ideal the generation and detection of the state. The state is well approximated by a mixture of the odd and even cat states  $|\psi\rangle = (|\alpha_0\rangle \pm |-\alpha_0\rangle)/\sqrt{2}$  with  $|\alpha_0| \approx 0.93$ . The mixedness is a result of decoherence due to optical loss, which in particular suppresses the (off-diagonal) coherence terms  $|\pm\alpha_0\rangle\langle\mp\alpha_0|$ . Center column: Grown Schrödinger cat state with  $W_{\min,1} = -0.0046 \pm 0.0012$ , and mean photon number  $\approx 1.98$ . Right column: After two growing steps, the number of data points was too low for a statistically significant negativity. It's clear to see that the post-processing increased the amplitude  $|\alpha|$  of the state since the maxima in Q and Wigner functions drifted apart and the mean photon of the state after two breeding steps increases to  $\approx 3.94$ .

$\mathcal{P} = \text{Tr}[\hat{\rho}^2]$ , the Mandel  $Q$ -parameter  $Q_M = ((\hat{n}^2) - \langle\hat{n}\rangle^2)/\langle\hat{n}\rangle - 1$  [34], which is negative when the state exhibits sub-Poissonian photon number distribution, the minimum value of Wigner function of the state  $W_{\min}$ , and maximum fidelity  $F$  of the state with a pure squeezed single-photon state. Error bars indicate one standard deviation. The statistical errors were determined by bootstrapping. We emphasize that we do not compensate for any losses during the state reconstruction and during the subsequent evaluation of the state parameters from the reconstructed density matrix. The observed values of state purity and fidelity can be attributed to losses and noise, and the state can be approximately modeled as mixed photon-subtracted squeezed thermal state.

### 3. GENERATING “MEASUREMENT” DATA ON GROWN STATES

Measurement data from Q-function-homodyning can be post-processed to generate “measurement” data from amplified states [35]. The advantage compared to a hardware-based approach [9,21,36] is groundbreaking. The data is indistinguishable, but neither doubling the quantum state generation hardware is required nor the integration of quantum memories. Most impor-

tantly, the success probability of this generally probabilistic approach is maximal, i.e., as good as what is achievable by the integration of perfect quantum memories [37].

We used the measured ensemble data of our microscopic Schrödinger cat state and probabilistically created reduced ensemble data as measured on states after one and two iterations of the breeding protocol. For perfect superpositions of two coherent states at the input, the protocol would result in growing of the amplitude of the cat state by a factor of  $\sqrt{2}$  after each iteration of the protocol. When a pure photon-subtracted squeezed vacuum is instead employed as an input of the protocol, one obtains a specific squeezed superposition of vacuum and two-photon Fock states after the first iteration of the protocol, and a specific squeezed superposition of Fock states  $|0\rangle$ ,  $|2\rangle$ , and  $|4\rangle$  after two iterations of the protocol. Losses and noise present in the initial state however degrade the performance of the iterative breeding, and the state becomes more noisy after each breeding step.

The hardware-based growing uses overlapping of two copies of the state on a balanced beam splitter (BS) followed by the probabilistic generation of a trigger signal from one BS output port heralding the grown state in the other BS output port. Here, we emulated this procedure by “overlapping” the measurement data from two ensemble members on a virtual BS as follows:

$$\alpha_{j+} = \frac{1}{\sqrt{2}}(\alpha_j + \alpha_{j+1}), \quad \alpha_{j-} = \frac{1}{\sqrt{2}}(\alpha_j - \alpha_{j+1}), \quad (1)$$

**Table 1. Parameters of the Experimentally Generated State ( $m = 0$ ) and the States after One and Two Emulated Breeding Steps ( $m = 1, 2$ )<sup>a</sup>**

$m$	$\bar{n}$	$Q_M$	$\mathcal{P}$	$W_{\min}$	$F$
0	$1.08463 \pm 0.00007$	$-0.12722 \pm 0.0001$	$0.5113 \pm 0.00008$	$-0.09266 \pm 0.00007$	$0.6241 \pm 0.0001$
1	$1.9804 \pm 0.0011$	$-0.0028 \pm 0.0016$	$0.3680 \pm 0.0007$	$-0.0046 \pm 0.0012$	$0.4455 \pm 0.0019$
2	$3.936 \pm 0.015$	$0.157 \pm 0.022$	$0.326 \pm 0.010$	-	$0.404 \pm 0.027$

<sup>a</sup>Given are the states' mean photon number  $\bar{n}$ , Mandel  $Q$ -parameter  $Q_M$  [34], state purity  $\mathcal{P}$ , maximum negativity of the Wigner function  $W_{\min}$ , maximum fidelity  $F$  with squeezed Fock state  $|1\rangle$  ( $m = 0$ ), squeezed superpositions of Fock states  $|0\rangle$  and  $|2\rangle$  ( $m = 1$ ), and squeezed superposition of Fock states  $|0\rangle$ ,  $|2\rangle$ , and  $|4\rangle$  ( $m = 2$ ).

where  $\alpha_j = X_{\text{mode},j}^Q + iY_{\text{mode},j}^Q$  and  $\alpha_{j+1} = X_{\text{mode},j+1}^Q + iY_{\text{mode},j+1}^Q$  with  $1 \leq j \leq 6 \times 10^8$ . If the amplitude in the destructively interfering output by chance obeyed  $|\alpha_j|^2 < \bar{q}$ , where  $\bar{q}$  was a freely choosable hard boundary, “measurement” data on an enlarged state  $|\alpha_1| > |\alpha_0|$  emerged in terms of  $\alpha_{j+}$ .

The center column of Fig. 4 shows the ensemble result after one such growing step with  $\bar{q} = 0.025$ . Just 7,414,579 quadrature pairs were produced, which corresponded to a yield of approximately 1.2%. The amplitude increased to  $|\alpha_1| \approx 1.48$ . A small negativity value is still visible in the reconstructed Wigner function (center, bottom). Also this data is not corrected, and imperfections increased due to the two-copy interference in the post-processing. The ensemble size is generally halved by the interference/growing process. The strongest reduction in ensemble size, however, comes from the probabilistic growing process, whose success rate strongly depends on the value  $\bar{q}$ . The right column of Fig. 4 shows the result of two-step grown “measurement” data according to Eq. (1). Just 37,375 quadrature data pairs were produced, which corresponded to a yield of the second breeding step of approximately 0.5%. Again, the data is not corrected for any imperfections. Due to the low sample size, the reconstructed Wigner function shows large statistical noise, and no negativity can be claimed. Several key parameters of the states after one and two iterations of the breeding protocol are listed in Table 1. The observed decrease of state fidelity and purity is a consequence of losses and noise, whose detrimental effects get enhanced during the breeding. Further growth steps would be possible if a longer measurement period had provided a larger initial dataset. Of course, the state decoherence would also increase further with each growth step.

#### 4. SUMMARY AND CONCLUSION

Our work demonstrates a concept for the generation of tomographic measurement data of mesoscopic quantum-correlated states for cases where the physical generation of these states is not yet possible. The starting point for this is physically existing states with analog kind of quantum correlations of *microscopic* “size” having a quantum-correlated photon number of the order of one. We define “mesoscopic” as numbers of quantum-correlated photon counts of the order of ten.

We experimentally produced a microscopic optical Schrödinger cat state of the size of approximately one quantum-correlated photon in the established way [17,18]. Different from previous experiments we measured on each individual copy the full quantum information that was contained in the corresponding pair of non-commutative quadrature phases. This was possible by splitting each individual copy with a balanced beam splitter and measuring the two quantities simultaneously. The post-processing of the data emulated the optical interference of

two copies. The two emulated interference results corresponded to two complex-valued numbers. If one was below a threshold value, the other corresponded to a measurement value as taken after a growth process. The “measurement” data generated in this way was indistinguishable from those that would have been measured on optically existing grown states as realized in [9]. Our procedure did not represent a post-selection, as the threshold value did not result from the physical nature of the desired grown state. In our case, further growth steps could easily be added. The number of our iterative growth steps was two and only limited by the number of measured copies of the initial state, i.e., by the initial measuring time. With each emulated growth step, the ensemble size was not only halved, but further reduced depending on the threshold(s). Importantly, however, the probability of success was maximal, i.e., as good as can be achieved with perfect interference contrast and by integrating perfect quantum memories.

Since the grown state of our concept never exists, an implementation in quantum information processing is precluded, which is also the case with approaches to conditional generation of quantum states based on post-selection. Nevertheless, our concept does have an important application. Since our concept includes a variable data post-processing structure that can be easily adapted and optimized, it provides a cost-effective way of benchmarking to determine the potentially optimal performance of a sophisticated quantum information protocol if it were physically implemented. The generation of mesoscopic quantum states of light by breeding is currently a rather hot topic in the context of optical quantum computing [7]. Our approach could be used to benchmark-related hardware to see if it can even in principle perform the desired task and generate states of required quality.

**Funding.** ERDF of the European Union and by “Fonds of the Hamburg Ministry of Science, Research, Equalities and Districts (BWFGB)”; Deutsche Forschungsgemeinschaft (757/7-1); Consejo Nacional de Investigaciones Científicas y Técnicas; Grantová Agentura České Republiky (21-23120S).

**Acknowledgment.** Until 2021, it was financed by the Deutsche Forschungsgemeinschaft (DFG)–SCHN 757/7-1. L.R. was supported by the Consejo Nacional de Investigaciones Científicas y Técnicas (CONICET). J.F. acknowledges support by the Czech Science Foundation. The dead and alive cats were produced by Kim-Melina Bertram.

D.A., J.F., and R.S. planned the experiment. J.G., F.P., M.L., S.G., D.A., L.R., and B.H. built and performed the experiment. F.P., S.G., and J.F. provided the theoretical analysis. R.S., J.F., and S.G. prepared the manuscript.

**Disclosures.** The authors declare no competing interests.

**Data availability.** Data may be obtained from the authors upon reasonable request.

## REFERENCES

1. J. Abadie, B. P. Abbott, R. S. Abbott, *et al.*, "A gravitational wave observatory operating beyond the quantum shot-noise limit," *Nat. Phys.* **7**(12), 962–965 (2011).
2. D. Ganapathy, W. Jia, M. Nakano, LIGO O4 Detector Collaboration, *et al.*, "Broadband quantum enhancement of the LIGO detectors with frequency-dependent squeezing," *Phys. Rev. X* **13**(4), 041021 (2023).
3. T. Gehring, V. Händchen, J. Duhme, *et al.*, "Implementation of continuous-variable quantum key distribution with composable and one-sided-device-independent security against coherent attacks," *Nat. Commun.* **6**, 8795 (2015).
4. W. Zhang, T. van Leent, K. Redeker, *et al.*, "A device-independent quantum key distribution system for distant users," *Nature* **607**(7920), 687–691 (2022).
5. M. V. Larsen, X. Guo, C. R. Breum, *et al.*, "Deterministic generation of a two-dimensional cluster state," *Science* **366**(6463), 369–372 (2019).
6. K. Fukui and S. Takeda, "Building a large-scale quantum computer with continuous-variable optical technologies," *J. Phys. B: At. Mol. Opt. Phys.* **55**(1), 012001 (2022).
7. H. Aghaee Rad, T. Ainsworth, R. N. Alexander, *et al.*, "Scaling and networking a modular photonic quantum computer," *Nature* **638**(8052), 912–919 (2025).
8. D. Gottesman, A. Kitaev, and J. Preskill, "Encoding a qubit in an oscillator," *Phys. Rev. A* **64**(1), 123101 (2001).
9. D. V. Sychev, A. E. Ulanov, A. A. Pushkina, *et al.*, "Enlargement of optical Schrödinger's cat states," *Nat. Photon.* **11**(6), 379–382 (2017).
10. S. Konno, W. Asavanant, F. Hanamura, *et al.*, "Logical states for fault-tolerant quantum computation with propagating light," *Science* **383**(6680), 289–293 (2024).
11. P. Zapletal, T. Darras, H. Le Jeannic, *et al.*, "Experimental Fock-state bunching capability of non-ideal single-photon states," *Optica* **8**(5), 743–748 (2021).
12. R. Schnabel, "Squeezed states of light and their applications in laser interferometers," *Phys. Rep.* **684**, 1–51 (2017).
13. H. Vahlbruch, M. Mehmet, K. Danzmann, *et al.*, "Detection of 15 dB squeezed states of light and their application for the absolute calibration of photoelectric quantum efficiency," *Phys. Rev. Lett.* **117**(11), 110801 (2016).
14. K. Vogel and H. Risken, "Determination of quasiprobability distributions in terms of probability distributions for the rotated quadrature phase," *Phys. Rev. A* **40**(5), 2847–2849 (1989).
15. G. Breitenbach, S. Schiller, and J. Mlynek, "Measurement of the quantum states of squeezed light," *Nature* **387**(6632), 471–475 (1997).
16. M. Dakna, T. Anhut, T. Opatrny, *et al.*, "Generating Schrödinger-cat-like states by means of conditional measurements on a beam splitter," *Phys. Rev. A* **55**(4), 3184–3194 (1997).
17. A. Ourjoumtsev, R. Tualle-Brouri, J. Laurat, *et al.*, "Generating optical Schrödinger kittens for quantum information processing," *Science* **312**(5770), 83–86 (2006).
18. J. Neergaard-Nielsen, B. Melholt Nielsen, C. Hettich, *et al.*, "Generation of a superposition of odd photon number states for quantum information networks," *Phys. Rev. Lett.* **97**(8), 083604 (2006).
19. A. Ourjoumtsev, A. Dantan, R. Tualle-Brouri, *et al.*, "Increasing entanglement between Gaussian states by coherent photon subtraction," *Phys. Rev. Lett.* **98**(3), 030502 (2007).
20. W. Asavanant, K. Nakashima, Y. Shiozawa, *et al.*, "Generation of highly pure Schrödinger's cat states and real-time quadrature measurements via optical filtering," *Opt. Express* **25**(26), 32227 (2017).
21. A. P. Lund, H. Jeong, T. C. Ralph, *et al.*, "Conditional production of superpositions of coherent states with inefficient photon detection," *Phys. Rev. A* **70**(2), 020101 (2004).
22. C. Y. Lu, X. Q. Zhou, O. Gühne, *et al.*, "Experimental entanglement of six photons in graph states," *Nat. Phys.* **3**(2), 91–95 (2007).
23. Y. F. Huang, B. H. Liu, L. Peng, *et al.*, "Experimental generation of an eight-photon Greenberger-Horne-Zeilinger state," *Nat. Commun.* **2**(1), 546 (2011).
24. E. Arthurs and J. L. Kelly, "On the simultaneous measurement of a pair of conjugate observables," *Bell System Techn. J.* **44**(4), 725–729 (1965).
25. N. G. Walker and J. E. Carroll, "Multiport homodyne detection near the quantum noise limit," *Opt. Quant. Electron.* **18**(5), 355–363 (1986).
26. V. Scarani, H. Bechmann-Pasquinucci, N. J. Cerf, *et al.*, "The security of practical quantum key distribution," *Rev. Mod. Phys.* **81**(3), 1301–1350 (2009).
27. K. Husimi, "Some formal properties of the density matrix," *Proc. Phys. Math. Soc. Jpn.* **22**(4), 264–314 (1940).
28. Z. Hradil, "Quantum-state estimation," *Phys. Rev. A* **55**(3), R1561–R1564 (1997).
29. M. Ježek, J. Fiurášek, and Z. Hradil, "Quantum inference of states and processes," *Phys. Rev. A* **68**(1), 012305 (2003).
30. A. I. Lvovsky, "Iterative maximum-likelihood reconstruction in quantum homodyne tomography," *J. Opt. B: Quant. Semiclass. Opt.* **6**(6), S556–S559 (2004).
31. A. Aspect, P. Grangier, and G. Roger, "Experimental tests of realistic local theories via Bell's theorem," *Phys. Rev. Lett.* **47**(7), 460–463 (1981).
32. M. Giustina, A. Mech, S. Ramelow, *et al.*, "Bell violation using entangled photons without the fair-sampling assumption," *Nature* **497**(7448), 227–230 (2013).
33. B. Hensen, H. Bernien, A. E. Dréau, *et al.*, "Loophole-free Bell inequality violation using electron spins separated by 1.3 kilometres," *Nature* **526**(7575), 682–686 (2015).
34. L. Mandel, "Squeezing and photon antibunching in harmonic generation," *Opt. Commun.* **42**(6), 437–439, Eq. (12) (1982).
35. J. Fiurášek and N. J. Cerf, "Gaussian postselection and virtual noiseless amplification in continuous-variable quantum key distribution," *Phys. Rev. A* **86**(6), 1–5 (2012).
36. J. S. Lagaout, A. Neergaard-Nielsen, I. Rigas, *et al.*, "Amplification of realistic Schrödinger-cat-state-like states by homodyne heralding," *Phys. Rev. A* **87**(4), 043826 (2013).
37. D. Abdelkhalik, M. Syllwasschy, N. J. Cerf, *et al.*, "Efficient entanglement distillation without quantum memory," *Nat. Commun.* **7**(1), 11720 (2016).